MEASUREMENT OF THE HEAT TRANSFER IN A GENERIC TURBINE INTERNAL COOLING PASSAGE

Charles W. Booten
Mechanical Engineering Department,
Stanford University
Stanford, California 94305, USA
booten@stanford.edu

John K. Eaton
Mechanical Engineering Department,
Stanford University
Stanford, California 94305, USA
eaton@vk.stanford.edu

ABSTRACT

The steady state heat transfer characteristics were measured in a stationary generic four passage serpentine model of a turbine blade internal cooling passage. Turbulators were used to enhance heat transfer with a pitch to height ratio of 8.5:1 and blockage ratio of 0.1. Heated copper elements were placed at certain locations throughout the model with the ability to apply a known heat flux on the copper and measure the thermal response in the passages with thermocouples embedded flush with the passage wall. Nusselt numbers were calculated and compared with the literature.

INTRODUCTION

Inaccurate knowledge of the distribution of the heat transfer rates in turbine internal cooling passages is a major factor in the uncertainty of turbine-blade metal temperature and lifespan prediction. Figure 1 shows a sample turbine blade with internal cooling passages. The air that flows through these passages is bled from the high pressure compressor, bypassing the combustor and enters through the root of the blades. In modern turbine blades there are typically three to four sets of cooling passages, one each for the leading and trailing edges and one to two sets of mid-chord passages. These serpentine passages are extremely complicated including multiple separation regions, strong secondary flows, and substantial roughness in the form of ribs (also referred to as turbulators).

The complicated geometry makes detailed measurements and CFD simulations difficult. Experimentally it is difficult to install instrumentation to provide spatially resolved measurements in complex internal flows. In the case of CFD, the grid must be extremely complex to resolve the separation regions behind each of the many ribs and both flow separation and strong secondary flows offer significant challenges for turbulence models. Because detailed heat transfer information is rarely available, turbine analysis systems often assign a single value of the heat transfer coefficient for the entire passage using empirical correlations.

The goal of this work is to provide detailed heat transfer measurements of a generic ribbed serpentine passage that captures much of the complexity of a real passage but eliminates such effects as variable passage cross section, passage twist, and film cooling discharge. These measurements are conducted in the same geometry and in the same Reynolds number range as used by Elkins et al. (2004) for fluid mechanics measurements. They used magnetic resonance velocimetry to provide three-component mean velocity measurements throughout a four-passage ribbed serpentine geometry.

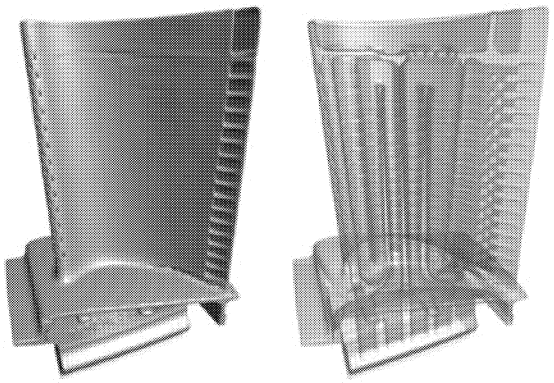

Figure 1: Turbine blade with serpentine cooling passages. Reproduced from Lindstrom (2000).

This experiment provides intermediate spatial resolution between typical heat exchanger type tests which supply a single average heat transfer coefficient for the entire passage and fully resolved tests which use a constant heat flux surface and optical temperature measurement. Fabricating a constant heat flux surface for this entire geometry would be very difficult. Hacker and Eaton (1997) and Booten and Eaton (2005) have shown that measurement of the heat transfer rate from discrete elements along with simultaneous measurement of the thermal wake of the heated element provides sufficient information to characterize the heat transfer over the entire surface. The advantage of this approach over other methods is the ability to make accurate heat transfer measuremnts quickly. Previously mentioned procedures typically have only one of those characteristics.

EXPERIMENTAL APPARATUS

Heat transfer measurements were performed in a generic serpentine passage model called the Stanford Generic Turbine Internal Passage (SGTIP) model, shown in Fig. 2. There are four square section passages, 20mm x 20mm, each with angled ribs (turbulators) with square cross-section (2mm x 2mm) on two opposing walls; only the ribs on one wall are visible in the figure. There were two types of corners, one round and two square, that are representative of the range of corner variations seen in actual serpentine cooling passages.

The model was designed to adhere closely to industry design practices regarding rib placement (10 per passage per wall), rib pitch to height ratio (8.5:1) and blockage ratio, defined as the rib height over the passage hydraulic diameter (0.1). The ribs are angled 45° to the passage axis and they are staggered such that the top and bottom ribs are equidistant from adjacent ribs on the opposite wall. The wall thickness between passages is 8mm. The model was fabricated using DSM Somos Watershed resin in a stereolithography system providing excellent resolution of the geometry to within approximately 0.051mm. The apparatus upstream of this test section, shown in Fig. 3, includes a compressed air supply, a pressure regulator, a laminar flow meter, a 1.8 meter long development tube, and a short transition nozzle blending the round tube flow into the square cross section serpentine passage. The development tube was bored to 32.8 mm (±0.05 mm) and honed to a surface roughness of 16 microinches to insure hydrodynamically-fully-developed pipe flow at the inlet to the test section.

Heat transfer was measured using discrete heated elements placed at 7 locations on the straight sections of the passage and at 6 locations in the corners as shown in Fig. 2. In

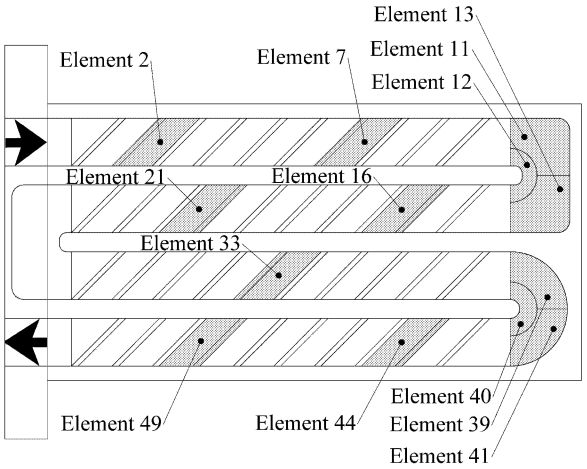

Figure 2: Four passage serpentine, SGTIP, model with heated copper locations.

the straight passage experiments, an 'element' refers to one rib pitch on one wall with turbulators. An example of one of these elements is the shaded copper element in Fig. 4. All elements in the straight sections of the passages are geometrically identical except the elements adjacent to the corners (e.g. elements 10 and 14 in Fig. 2). The elements adjacent to the corners are not considered in this paper and will not be mentioned further. The corner elements have no turbulators on them and are of various sizes depending on location. The measurement resolution is much higher than the element

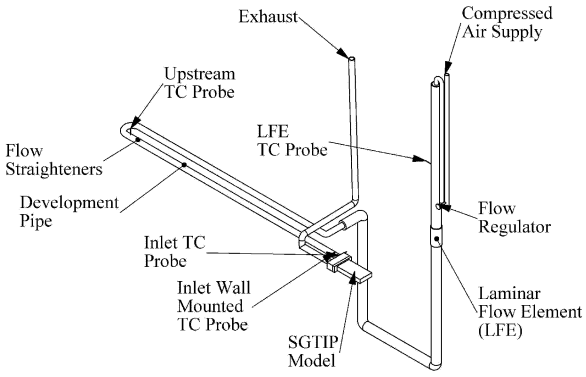

Figure 3: Schematic of the experimental apparatus.

resolution. The thermocouple locations in Fig. 4 show that there are between 4 and 12 thermocouples per element in the straight section while the corner elements have between 6 and 7. The thermocouple numbering scheme for the straight section instrumented piece is shown in Fig. 5. The heated copper element is shaded as in Fig. 4.

A four-rib-pitch section of one passage wall was instrumented and mounted in a moveable plug such that the same instrumented plug could be used to perform the measurements at all the desired locations in the straight sections of the model. The surface side of this plug, as well as thermocouple locations, are shown in Fig. 4. The main flow in Fig.

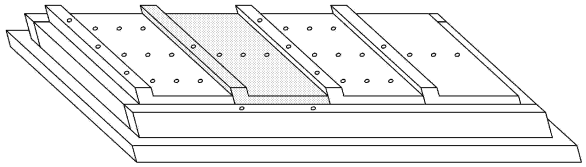

Figure 4: Removable instrumented plug for taking heat transfer measurements. The small circles indicate thermocouple locations.

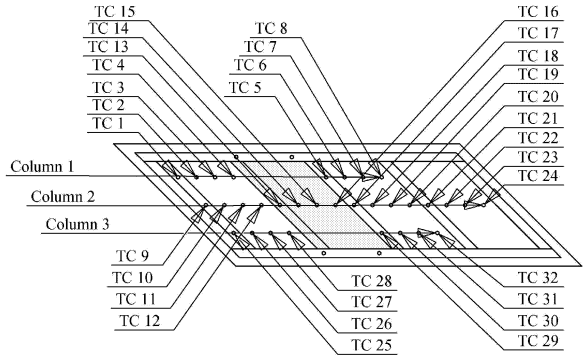

Figure 5: Thermocouple numbers for straight section removable plug.

4 is moving from left to right The heated element is shaded and was made of copper machined to be geometrically identical to the test geometry. The copper in Fig. 4 is one rib pitch long in the axial direction (16.98mm) and covers one wall. The copper elements around the corners can be seen schematically in Fig. 2; they also were geometrically identical to the wall section they replaced. Each copper element was heated using a pair of thermofoil heaters and the temperature

was measured using sets of 4-12 embedded thermocouples per rib pitch as can be seen in Fig. 4. The thermocouples were embedded in the passage walls such that they were flush with the inner wall surface.

The element sizes were chosen to roughly correspond to different flow conditions over the corner surface while maintaining an ability to easily instrument and heat the pieces. Elkins et al. (2004) used magnetic resonance velocimetry (MRV) and particle image velocimetry (PIV) comparisons to clearly show that the mean velocity magnitude increases near the inside radius of the corner. This increase in velocity is the basis of the design decision that led to separating the corners into inner and outer components. The outer section was separated into upstream and downstream sections because at different Reynolds numbers the momentum in the flow causes impingement to occur at different locations; two elements allows for better resolution of this effect while maintaining some experimental expediency.

A known heat flow was supplied to one of these copper elements per experiment. The thermocouples were monitored and determined to be at steady state if the standard deviation in 30 successive readings of 32 samples at each location was less than 0.02 °C. The minimum time for this was ∼30 minutes, however, in practice steady state was usually reached after approximately 2 hours at a given set of flow conditions. The steady-state thermal response of the wall was then recorded from 1000 samples from each thermocouple. This was repeated for all copper element locations for 15,000≤Re≤55,000. The entire model and development tube were insulated using polyethylene and polystyrene insulation (k ∼ 0.036 $^{W}/_{mK}$ for both materials). The minimum thickness of the insulation is 76 mm, with insulation up to 100 mm in certain locations to approximate adiabatic thermal boundary conditions everywhere except on the copper elements.

EXPERIMENTAL RESULTS

Adiabatic Wall Temperature

The adiabatic wall temperature, T_{aw}, can differ significantly from the test section inlet temperature; this is especially true for the highest Reynolds numbers where the local Mach numbers can exceed 0.2. Therefore T_{aw} was measured with no heat addition at all locations and Reynolds numbers to provide a correct reference temperature for heat transfer calculations. A sample of the adiabatic wall temperature for all thermocouples measured with the copper on the instrumented piece located at element 44 is shown in Fig. 6. The adiabatic wall temperature is within ±0.06°C of the inlet stagnation temperature at all measurement locations for the lowest Reynolds number. However, T_{aw} drops below the inlet temperature by around 0.2°C for the intermediate Reynolds number case and by as much as 0.6°C for the high Reynolds number case. The peak Mach number is at least 0.2 due to the highly non-uniform flow in the passage. This is corroborated by data presented by Elkins et al. (2004). Assuming a recovery factor of $Pr^{1/3}$ and a freestream Mach number of 0.12, a reduction in the adiabatic wall temperature of about 0.75°C below stagnation temperature is expected. This rough calculation confirms that the measured T_{aw} is in the expected range.

The accuracy of the thermocouple measurements was verified using a thermistor. The thermistor was placed between

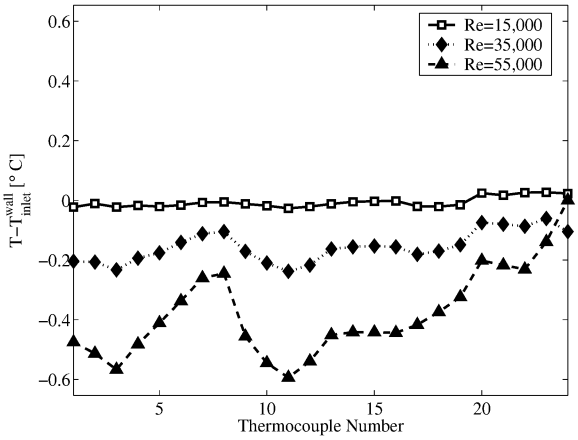

Figure 6: Difference between adiabatic wall temperature and inlet temperature for all Reynolds numbers on elements 43-46.

thermocouples at the copper element location when measuring the adiabatic wall temperature . The copper element was also replaced in order to eliminate any possible effects it might have on the adiabatic wall temperature. A sample of the recorded temperatures for the thermistor and the two adjacent thermocouples is shown in Fig. 7. This demonstrates

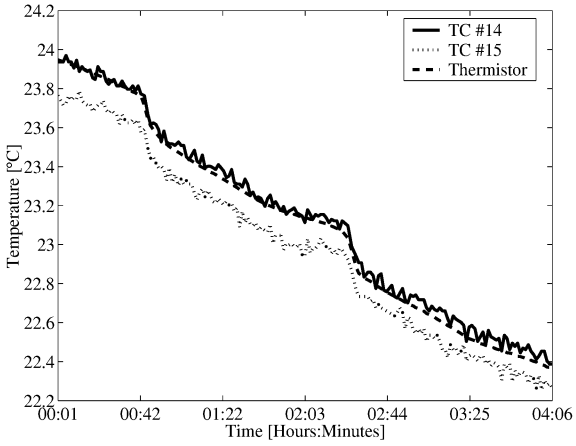

Figure 7: Temporal measurement of thermistor and adjacent thermocouples on element 44.

that the thermocouple readings are consistent with the thermistor within 0.2°C. The sharp decreases in temperature in Fig. 7 around times 00:42 and 02:20 correspond to increases in Reynolds number . The slower trend of decreasing temperature is due to daily fluctuations in ambient temperature.

Thermal Response

The steady state thermal response for Reynolds number = 35,000 with element 33 heated is shown in Fig. 8. Here x is measured along the same direction as the mean flow, beginning at the leading edge of the instrumented plug, which corresponds to the left edge of the rib of the left element in Fig. 4. The ribs are all at an angle of 45° to the flow so the axial position corresponding to x = 0 depends on the distance from the side walls. This coordinate system means that thermocouples 1, 9 and 25 all have the same x location, as do thermocouples 2, 10 and 26, etc. The x location of the ther-

mocouples was non-dimensionalized in Fig. 8, and the heated copper element is located between 1.6e-4≤x^+≤3.2e-4.

The measured temperature on the copper element is nearly uniform as expected. The temperature distribution is fairly uniform parallel to the ribs as well. The exception to this is just downstream of the copper element. The temperature rise is greater near the separation wall than the impingement wall. The separation wall is the non-ribbed wall adjacent to the leading edge of the ribs. The impingement wall is the other non-ribbed wall. They are so-called because the flow on the ribbed walls tends to separate from one and impinge on the other. As the flow progresses down the passage it is swept towards the trailing edge of the ribs, which are adjacent to the impingement wall. This can be seen by looking at Fig. 9 (reproduced from Iaccarino et al. 2003) which shows the velocity magnitude in the centerplane of the channels. In addition to demonstrating how the mean flow moves towards the impingement wall, Fig. 9 also shows the separation region downstream of the corners that creates large velocity profile distortion that could change the value of the recovery factor and Mach number in localized areas.

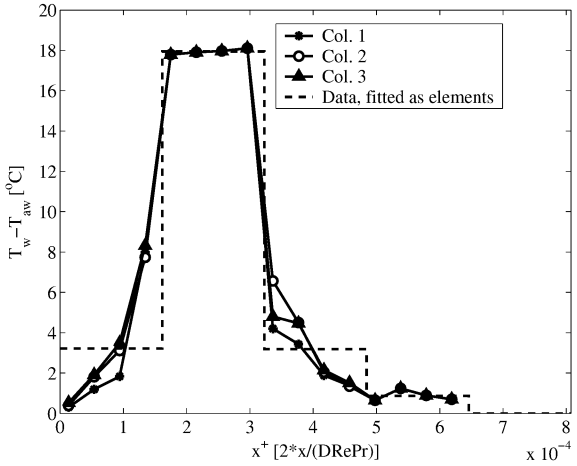

Figure 8: Steady state thermal response for element 33, Re = 35,000

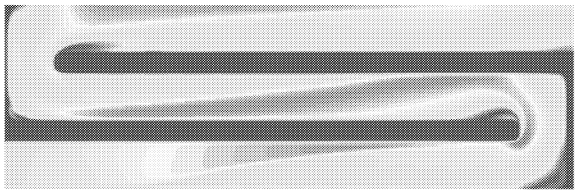

Figure 9: Velocity magnitude in channel centerplane from Iaccarino et al. (2003), Re = 35,000

There are two other important characteristics of the footprint, or thermal response in Fig. 8. One is that the secondary flow and turbulent mixing are so strong that the heat that is transferred into the flow is well mixed by the time it has travelled two rib pitches downstream of the heated element. Thus, measurement of the thermal footprint of a heated element requires only a short region of instrumented test wall. There is also substantial heating upstream of the copper element. This is caused by recirculation drawing heat from the rib on the upstream end of the copper element and transferring it to the wall upstream. This effect is still substantial even after conduction losses from the copper are corrected for.

The temperature rise averaged over the elements gives a good indication of both the heat transfer coefficient at the heated element plus the strength of the thermal wake. These averages allow quick comparison between the various element locations. Figure 10 shows the temperature rise divided by the heat transfer rate for each of the seven heated elements. The vertical lines represent a discrete element number at which all corresponding data were measured. The temperature rise is

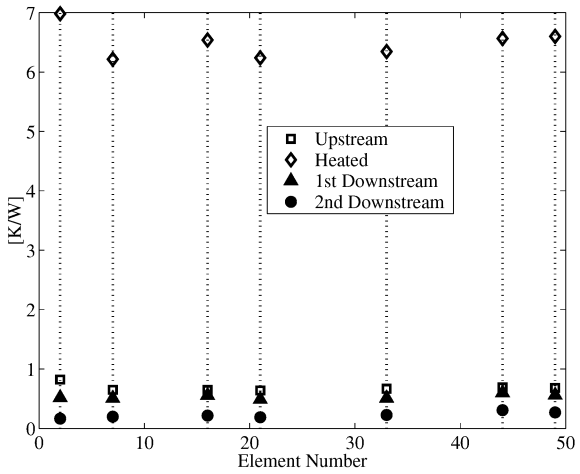

Figure 10: Thermal response at all measured locations per unit power supplied to copper element, Re = 35,000.

nearly the same for each element, regardless of its position in the passage. This clearly demonstrates that the periodic rib structure dominates the heat transfer behavior.

Also shown are the temperatures averaged over the first upstream, and the two downstream elements. These also show almost no sensitivity to position in the passage, demonstrating that the thermal footprint at multiple locations can be well approximated (within 7% on the heated element) by only measuring it at one or two locations throughout the serpentine passages.

Nusselt Number Measurements

The Nusselt number was measured by first taking the steady state thermal response of all thermocouples on the copper surface and obtaining an average temperature rise over the copper element. The applied heat flow to the copper was obtained by subtracting the estimated conduction losses from the nominal power supplied to the copper. The Nusselt number was calculated according to

$$Nu = \frac{\frac{\dot{Q}}{A_s \Delta T} D}{k} \tag{1}$$

where $\dot{Q}$ is the net heat flow, A_s is the surface area of the copper element, including the area of the rib, k is the thermal conductivity of the air, D is the passage hydraulic diameter and

$$\Delta T = T_{wall} - T_{adiabatic\ wall}. \tag{2}$$

The conduction losses from the copper result in non-adiabatic boundary conditions immediately upstream and downstream of the copper. This has some effect on the Nusselt number on

the copper element that is not accounted for in this formulation; however, the Nusselt number can be adjusted to account for the actual thermal boundary conditions using the analysis for internal flow heat transfer in Booten and Eaton (2005).

Conduction Losses. The conduction losses from the heated copper element were estimated by modeling a section of the SGTIP model using FLUENT, a commercial computational fluid dynamics code to calculate conduction in the solid. This heat loss was used to adjust the $\dot{Q}$ in Eq. 1. The boundary conditions that were used in place of the fluid were temperature measurements on the heated elements and convective boundary conditions on all other elements adjacent to the fluid. The outer boundaries were considered to be adiabatic.

The values for the convective heat transfer coefficients that were specified were based on the ranges reported in the literature. This approximation of constant heat transfer coefficients on surfaces in the model has small effects on the overall Nusselt numbers that were computed because the conduction losses are relatively small compared to the amount of heat input and they are relatively insensitive to changes in the heat transfer coefficient boundary conditions. Changes up to $\pm 30\%$ in heat transfer coefficient boundary condition values result in a change in the Nusselt numbers of $\leq 7\%$ for all Reynolds numbers and locations.

Straight Sections. The Nusselt numbers for the straight sections were compared to Nusselt numbers for constant wall heat flux from the literature as shown in Fig. 11. These Nusselt numbers are nominally measured using constant heat flux boundary conditions with a step in wall heat flux beginning at the upstream edge of the element. The actual thermal boundary conditions in these experiments are somewhat different due to the experimental techniques often employed. Typically a section of wall is replaced with copper so that the flow is exposed to a constant wall temperature over that section. The thermal boundary conditions are actually for heat flux; a known heat flux is being supplied over the copper element with the approximation of adiabatic walls everywhere else. There is very good agreement with the literature over the entire range of Reynolds numbers measured even though the literature encompasses large variations in passage diameter, rib pitch to height ratio, rib blockage ratio, rib angle and stagger, corner design and methods of heating.

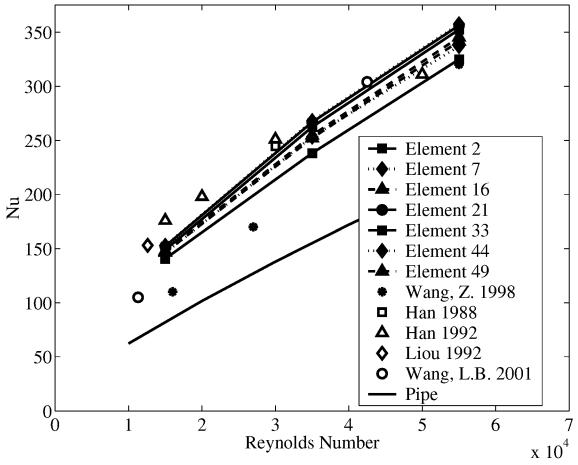

Figure 11: Nusselt number averaged over each heated element in straight section locations

The thermally fully developed Nusselt number was calculated using the analysis presented in Booten and Eaton (2005) so that it represents the Nusselt number for the copper element given a constant wall heat flux over the entire wall. The mean thermally fully developed Nusselt number for all straight sections was calculated and compared with fully developed Nusselt numbers in the literature and is shown in Fig. 12.

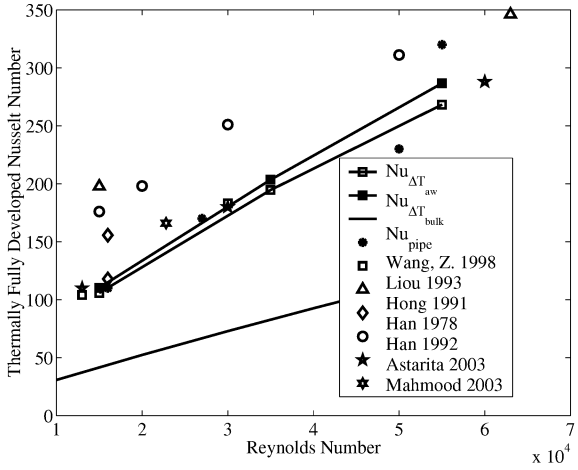

Figure 12: Thermally fully developed Nusselt number averaged over each heated element in straight section locations

There are two methods for calculating Nu_{FD}. The methods differ by how ΔT is defined in Eq. 2. It is common in the literature to use

$$\Delta T = (T_{wall} - T_{bulk}). \tag{3}$$

The Nusselt number defined using this ΔT is $Nu_{\Delta T_{bulk}}$. However, it is more appropriate to use

$$\Delta T = (T_{wall} - T_{adiabatic\ wall}) \tag{4}$$

to calculate the Nusselt number denoted as $Nu_{\Delta T_{aw}}$. This allows easier use of the superposition technique reported in Booten and Eaton (2005) to characterize heat transfer in internal passages. Both methods for calculating the Nusselt number are used in Fig. 12 for comparison and show very good agreement with the literature.

Corner Sections. The corners of the SGTIP model have significantly different flow and thermal characteristics than the straight sections. Separate measurements were performed using the same basic experimental technique as for the straight sections, except with different sized elements, as shown in Fig. 2.

The local Nusselt number on each corner element is plotted versus Reynolds number in Fig. 13. It is clear that the elements near the inside of the corners (elements 12 and 40) have a much higher heat transfer rate, due to the higher freestream velocities than near the outside of the corners. The Nusselt number on the downstream outer element on the square corner increases significantly slower than the upstream outer element

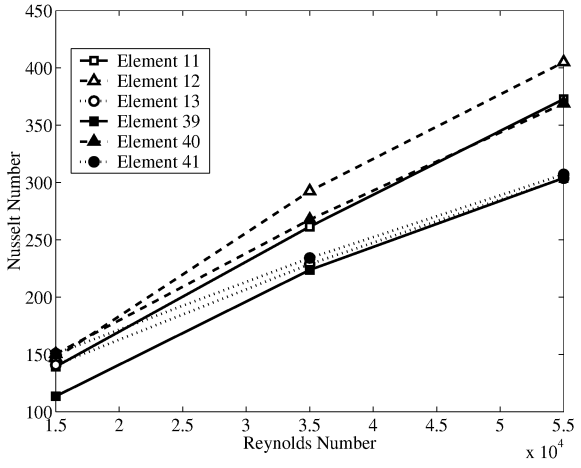

Figure 13: Nusselt number on corner elements vs. Reynolds number

with Reynolds number. This is because the flow produces a larger separation bubble at higher Reynolds number . This causes the impingement of the flow to be more directly on the upstream outer element than the downstream outer element which increases the heat transfer upstream relative to downstream locations. A similar trend is seen with the round corner, except it is less extreme because the rounded outer surface tends to sweep the flow around the corner better than the square corner.

CONCLUSIONS

This work has applied a method for quickly measuring the thermal characteristics inside a generic serpentine cooling passage model that is representative of those found in modern turbine blades. The thermal response to heating of a finite section of the passage wall was measured with intermediate spatial resolution using embedded thermocouples . This technique can be extended for calculating heat transfer coefficients that are valid for arbitrary thermal boundary conditions.

Ongoing work includes measuring the pressure distribution in the passages and around the corners and implementation of heat transfer into an immersed boundary condition RANS CFD code (IBRANS) for prediction of the thermal characteristics in serpentine passages.

ACKNOWLEDGEMENTS

This work was supported by GE Aircraft Engines and through the National Defense Science and Engineering Graduate Fellowship. The authors would also like to thank Prof. Ryan Wicker for his contributions of the rapid prototyping models used in the experiments.

REFERENCES

Booten, C.W., Eaton, J.K., 2005 "Discrete Green's Function Measurements in Internal Flows" *ASME Journal of Heat Transfer*, Accepted for Publication.

Elkins C.J., Markl M., Iyengar A., Wicker R., Eaton J.K., 2004 "Full Field Velocity and Temperature Measurements Using Magnetic Resonance Imaging in Turbulent Complex Internal Flows," in press *International Journal of Heat and Fluid Flow*.

Hacker, J.M., Eaton, J.K., 1997 "Measurements of Heat Transfer in a Separated and Reattaching Flow with Spatially Varying Thermal Boundary Conditions," *International Journal of Heat and Fluid Flow*, Vol. 18, No. 1, pp 131-141.

Han, J.C., Glicksman, L.R., Rohsenow, W.M., 1978 "An Investigation of Heat Transfer and Friction for Rib-Roughened Surfaces", *International Journal of Heat and Mass Transfer*, Vol. 21, pp. 1143-1156.

Han, J.C., 1988 "Heat Transfer and Friction Characteristics in Rectangular Channels With Rib Turbulators", *ASME Journal of Heat Transfer*, Vol. 110, pp. 321-328.

Han, J.C., Zhang, Y.M., Lee, C.P., 1992 "Influence of Surface Heat Flux Ratio on Heat Transfer Augmentation in Square Channels With Parallel, Crossed, and V-Shaped Angled Ribs", *Journal of Turbomachinery*, Vol. 114, pp. 872-880.

Hong, Y.J., Hsieh, S.S., 1991 "An Experimental Investigation of Heat Transfer Characteristics for Turbulent Flow over Staggered Ribs in a Square Duct", *Experimental Thermal and Fluid Science*, Vol. 4, pp. 714-722.

Hsu, C., 1968 "Exact solution to entry-region laminar heat transfer with axial conduction and the boundary condition of the third kind", *Chemical Engineering Science*, Vol. 23 pp. 457-468.

Iaccarino, G., Kalitzin, G., Elkins C.J., 2003 "Numerical and experimental investigation of the turbulent flow in a ribbed serpentine passage" Annual Research Briefs, Center for Turbulence Research pp. 415-426.

Kays, W.M., Crawford, M.E., 1993 *Convective Heat and Mass Transfer* McGraw-Hill, 3rd ed.

Lindstrom, P., 2000 "Out-of-Core Simplification of Large Polygonal Models", *Proceedings, ACM SIGGRAPH 2000*, New Orleans, LA, pp. 259-262.

Liou, T.M., Hwang, J.J., 1992 "Developing Heat Transfer and Friction in a Ribbed Rectangular Duct With Flow Separation at Inlet", *ASME Journal of Heat Transfer*, Vol. 114, pp. 565-573.

Liou, T.M., Hwang, J.J., 1993 "Effect of Ridge Shapes on Turbulent Heat Transfer and Friction in a Rectangular Channel", *International Journal of Heat and Mass Transfer*, Vol. 36, no. 4, pp. 931-940.

Mahmood, G.I., Ligrani, P.M., Chen, K., 2003 "Variable Property and Temperature Ratio Effects on Nusselt Numbers in a Rectangular Channel With 45 Deg Anlgled Rib Turbulators", *ASME Journal of Heat Transfer*, Vol. 125, pp. 769-778.

Taslim, M.E., Lengkong, A., 1999 "45 deg Round-Corner Rib Heat Transfer Coefficient Measurements in a Square Channel", *Journal of Turbomachinery*, Vol. 121, pp. 272-280.

Vick, B., Beale, J.H., and Frankel, J.I., 1987 "Integral Equation Solution for Internal Flow Subjected to a Variable Heat Transfer Coefficient", *ASME Journal of Heat Transfer*, Vol. 109, no. 4, pp. 856-860.

Wang, Z., Ireland, P.T.,Kohler, P.T., Chew, J.W., 1998 "Heat Transfer Measurements to a Gas Turbine Cooling Passage with Inclined Ribs", *Journal of Turbomachinery*, Vol. 120, pp. 63-69.

Wang, L.B., Tao, W.Q., Wang, Q.W., Wong, T.T., 2001 "Experimental Study of Developing Turbulent Flow and Heat Transfer in Ribbed convergent/Divergent Square Ducts", *International Journal of Heat and Fluid Flow*, Vol. 22, pp. 603-613.